Topological Shape Matching using Multi-Dimensional Reeb Graphs

Yashwanth Ramamurthi
International Institute of Information Technology (IIIT)
Bangalore, Karnataka, India
yashwanth@iiitb.ac.in

Amit Chattopadhyay
International Institute of Information Technology (IIIT)
Bangalore, Karnataka, India
a.chattopadhyay@iiitb.ac.in

ABSTRACT

Shape matching or retrieval is an important problem in computer graphics and data analysis. Topological techniques based on Reeb graphs and persistence diagrams have been employed to obtain an effective solution in this problem. In the current paper, we propose an improved technique based on the multi-dimensional Reeb graph (MDRG) that captures the topology of a multi-field through a hierarchy of Reeb graphs in different dimensions. To capture the persistent features in a multi-field, a hierarchy of persistence diagrams is then constructed by computing a persistence diagram corresponding to each Reeb graph of the MDRG. Based on this representation, we propose a novel distance measure between two MDRGs by extending the bottleneck distance between two Reeb graphs. We show that the proposed measure satisfies the pseudo-metric and stability properties. The effectiveness of the proposed multi-field topology based measure is tested on the shape data as compared to scalar topology based measures. We use normalized eigenfunctions of the Laplace-Beltrami operator, in pairs, as the bivariate descriptors of the shapes. The performance of the proposed measure is compared with the well-known topology based measures in shape matching using Heat Kernel Signature, Wave Kernel Signature and Scale-Invariant Heat Kernel Signature.

CCS CONCEPTS

• **Computing methodologies** → **Shape analysis**; • **Mathematics of computing** → **Topology**.

KEYWORDS

Shape Matching, Multi-Field, Multi-Dimensional Reeb graph, Distance Measure

ACM Reference Format:
Yashwanth Ramamurthi and Amit Chattopadhyay. 2022. Topological Shape Matching using Multi-Dimensional Reeb Graphs. In *Proceedings of the Thirteenth Indian Conference on Computer Vision, Graphics and Image Processing (ICVGIP'22), December 8–10, 2022, Gandhinagar, India,* Soma Biswas, Shanmuganathan Raman, and Amit K Roy-Chowdhury (Eds.). ACM, New York, NY, USA, Article 6, 10 pages. https://doi.org/10.1145/3571600.3571606

ICVGIP'22, December 8–10, 2022, Gandhinagar, India

ACM ISBN 978-1-4503-9822-0/22/12…$15.00
https://doi.org/10.1145/3571600.3571606

1 INTRODUCTION

Shape matching plays an important role in many fields and has been used widely in image recognition, object retrieval, bioinformatics, medical diagnosis etc. Recent advancement in computer hardware and shape acquisition technology has led to an increasing volume of shape database. As a result, the development of efficient algorithms of shape comparison, for retrieving a similar query shape from a shape database or classifying shapes into different classes, are of utmost importance. The goal of shape retrieval is usually achieved by computing a similarity or distance measures between a pair of shapes. Thus, the main challenge in developing shape retrieval algorithms is to design effective similarity metrics using shape descriptors which are invariant to both non-rigid deformations (e.g. scaling, stretching or shape perturbation) and rigid deformations (e.g. three-dimensional rotation and translation) of the shapes. Various shape descriptors, such as the geodesic distance [18], Heat Kernel Signature (HKS) [36], Wave Kernel Signature (WKS) [3], Scale-Invariant Heat Kernel Signature (SIHKS) [5] etc., have been studied in the literature to capture important properties of shapes.

Recent developments of topological similarity measures between shapes (or data) has facilitated the understanding the relationships between the shape topologies. Hilaga et al. [18] proposed a topological similarity measure based on multi-resolution Reeb graphs and and showed its effectiveness in clustering shape data. Zhang et al. [41] computed the similarity between protein structures based on their multi-resolution dual contour trees. Tam et al. [37] used topological points and rings for capturing the topological and geometric features of a shape and compared shapes using an Earth Mover Distance. Sridharamurthy et al. [35] proposed a tree edit distance between merge trees and applied it in the problem of shape matching. Persistent homology theory [10, 17, 42] has provided a simple yet powerful technique to encode the topological information of a scalar field into a bar code or persistence diagram. Li et al. [21] computed the persistence diagrams of shapes corresponding to the spectral descriptors HKS, WKS, SIHKS and compared the technique with the bag-of-features model.

Recently, multi-field topology is getting wider attention because of its ability to capture richer topological features than scalar topology, as has been shown in various data analysis applications in computational physics and computational chemistry [2, 13, 25]. However, the application of multi-field topology in the shape matching problem requires further development in the representation of such topological features and finding effective distance measures between such representations. In the current work, we propose a novel distance measure between two shapes based on their multi-dimensional Reeb graphs (MDRG). The MDRG is a topological descriptor which captures the topology of a multi-field using a series

of Reeb graphs in different dimensions. To compare two MDRGs, we compute the persistence diagrams corresponding to the component Reeb graphs and find a distance between two such collections of Reeb graphs using the bottleneck distance. We show that the proposed distance measure is stable and satisfies the pseudo-metric property. We validate the effectiveness of the proposed distance measure in shape retrieval by comparing with well-known topological techniques using the SHREC 2010 dataset [22]. In the current paper, our contributions are as follows.

- We propose a novel distance measure between MDRGs based on the bottleneck distance between the component Reeb graphs of the MDRGs.
- We show the proposed distance measure satisfies the stability and pseudo-metric properties.
- We show the effectiveness in using pairs of eigenfunctions of the Laplace-Beltrami operator as shape descriptors and compare the results with the well-known topology based techniques for the case SHREC 2010 dataset.

Outline. In section 2, we discuss shape descriptors, topological tools and their applications in shape matching. Section 3 discusses the necessary background required to understand the proposed distance measure. In Section 4 we describe the proposed distance measure between MDRGs. In section 5 we show the experimental results of the proposed measure in the shape matching problem and finally in section 6 we draw a conclusion.

2 RELATED WORK

An increase of interest in the Laplace-Beltrami (LB) operator resulted in the evolution of various signatures to capture the features in a shape [27, 28]. Reuter et al. [26] proposed the shape DNA, where a shape is represented using the eigenvalues of the Laplace-Beltrami operator and was able to identify the shapes with similar poses. However, non-isometric shapes can have the same set of eigenvalues. This drawback is overcome by the Global Point Signature (GPS) [29], where the eigenfunctions are used along with the eigenvalues. However, this introduced the sign ambiguity problem to the eigenfunctions (see section 4.3.1 for more details), which was solved using the Heat Kernel Signature (HKS) [36]. However, the HKS consists of information from low frequencies. The suppression of high frequencies makes it difficult to detect microscopic features. This limitation was overcome in the Wave Kernel Signature (WKS)[3] by using band-pass filters instead of low-pass filters. Bronstein et al. [5] propose a scale invariant version of the Heat Kernel Signature (SIHKS) by using logarithmic sampling and Fourier transform. Recently, Zihao et al. [40] proposed a shape descriptor based on the probability distributions of the eigenfunctions of the LB operator and showed its effectiveness over SIHKS. In this paper, we measure distance between shapes by directly comparing the eigenfunctions of the LB operator and show its performance with respect to HKS, WKS and SIHKS.

Several shape matching techniques have been developed based on the scalar topology tools such as contour Tree [41], Reeb Graph [18], and Merge tree [35]. Li et al. [21] computed the persistence diagrams of shapes corresponding to the spectral descriptors HKS, WKS, SIHKS and compared the technique with the bag-of-features model. Kleiman et al. [19] present a method for computing region-level correspondence between a pair of shapes by obtaining a shape graph corresponding to each shape and then matching the nodes of shape graphs. Poulenard et al. [24] present a characterization of functional maps based on persistence diagrams along with an optimization scheme to improve the computational efficiency.

Recently, tools for capturing multi-field topology have been studied using the Jacobi set [14], Reeb Space [16], Mapper [34], Joint Contour Net [6], Multi-Dimensional Reeb Graph [7, 8], etc. Techniques for comparing multi-fields have been developed such as the bottleneck distance between persistence diagrams of multiscale mappers [12], distance between fiber-component distributions [2] and similarity between multi-resolution Reeb spaces (MRSs) [25]. In the current paper, we capture the topological features in a multi-field by computing the persistence diagrams of the Reeb graphs in an MDRG and develop a distance measure between two such MDRGs based on the bottleneck distance between the component Reeb graphs of the MDRGs. We evaluate the effectiveness of the proposed distance measure in the shape matching problem using the SHREC 2010 dataset [22].

3 BACKGROUND

In this section, we discuss the necessary background required to understand the proposed distance measure and feature descriptors used in the comparison of shapes.

3.1 Multi-Field Topology

Let $\mathbb{M}$ be a triangulated mesh of a compact d-manifold $\mathcal{M}$. A multi-field on $\mathbb{M}$ with r component scalar fields is defined as a continuous map $\mathbf{f} = (f_1, f_2, ..., f_r) : \mathbb{M} \rightarrow \mathbb{R}^r$. For a value $\mathbf{c} \in \mathbb{R}^r$, its inverse $\mathbf{f}^{-1}(\mathbf{c})$ is called a *fiber*. Each connected component of a fiber is a *fiber-component* [31, 33]. In particular, for a scalar field $f : \mathbb{M} \rightarrow \mathbb{R}$, the inverse of f corresponding to a point in the range is called a *level set* and each connected component of a level set is called a *contour*. The Reeb space of $\mathbf{f}$, denoted by $\mathcal{RS}_\mathbf{f}$, is the quotient space by contracting each fiber-component to a point [16]. In particular, the Reeb space of a scalar field $f : \mathbb{M} \rightarrow \mathbb{R}$ is known as the Reeb graph $\mathcal{RG}_f$, which is obtained by contracting each contour to a point and $\tilde{f} : \mathbb{M} \rightarrow \mathcal{RG}_f$ is the corresponding quotient map. [32]. Carr et al. [6] proposed the Joint Contour Net (JCN) data-structure, which is a quantized approximation of the Reeb space. For construction of the JCN of $\mathbf{f}$, the range of $\mathbf{f}$ is subdivided into a finite set of r-dimensional intervals. For each interval, the inverse of $\mathbf{f}$ is a *quantized fiber* and each connected component of a quantized fiber is a *quantized fiber-component* or *joint contour*. The JCN is a graph where a node corresponds to a joint contour and an edge between two nodes corresponds to the adjacency of the corresponding joint contours in the domain.

3.2 Multi Dimensional Reeb Graph

A multi-dimensional Reeb graph (MDRG) of a multi-field $\mathbf{f} = (f_1, ..., f_r) : \mathbb{M} \rightarrow \mathbb{R}^r$, proposed by Chattopadhyay et al. [7, 8], is the decomposition of the Reeb space (or a JCN) into a series of Reeb graphs in different dimensions. To construct the MDRG of $\mathbf{f}$, the Reeb graph $\mathcal{RG}_{f_1}$ of the function f_1 is computed. Each point $p \in \mathcal{RG}_{f_1}$ represents a contour C_p of f_1. For every $p \in \mathcal{RG}_{f_1}$ a Reeb

graph corresponding to the field f_2 is computed by restricting f_2 on C_p. This procedure is repeated by computing the Reeb graphs for the function f_i by restricting f_i on the contours corresponding to points in the Reeb graphs of f_{i-1}, where $2 \leq i \leq r$. In practice, the MDRG is constructed from a quantized approximation of the Reeb Space (JCN). Therefore, similar to the JCN, the MDRG also depends on the subdivision of the range. Each node in a Reeb graph of the MDRG corresponds to a *quantized contour* and the adjacency between quantized contours is represented by an edge in the Reeb graph. Figure 1 shows the JCN and MDRG corresponding to a bivariate field. In the current paper, we compute persistence diagrams corresponding to Reeb graphs in the MDRG and propose a distance to compare the collection of persistence diagrams of two MDRGs based on the bottleneck distance between Reeb graphs [4].

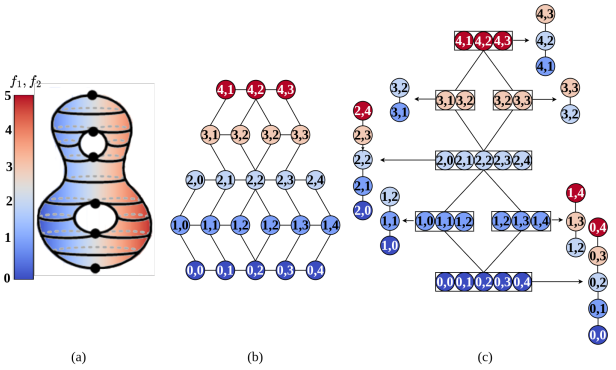

Figure 1: (a) A piecewise linear bivariate data over a double torus: The black curves depict the contours of the first field (f_1) and the mesh is colored based on the values of the second field (f_2), (b) JCN at 5×5 resolution: the coloring of the nodes are is based on the values of the first field, (c) MDRG computed using the algorithm in [8]: the coloring of the nodes in the first (second) dimension is based on the values of f_1 (f_2).

3.3 Persistence Diagram

In this paper, we give a brief introduction to the notion of *persistence diagrams* and refer the readers to [15, 42] for further details on persistent homology.

Let f be a continuous real-valued function defined on $\mathbb{M}$. For a value $a \in \mathbb{R}$, the sublevel set $\mathbb{M}_{\leq a}$ consists of the points in $\mathbb{M}$ with f-value less than or equal to a, i.e. $\mathbb{M}_{\leq a} = f^{-1}(-\infty, a]$. For $a \leq b$, the l-th homology groups of the sublevel sets $\mathbb{M}_{\leq a}$ and $\mathbb{M}_{\leq b}$ are connected by the inclusion map $f_l^{a,b} : H_l(\mathbb{M}_{\leq a}) \to H_l(\mathbb{M}_{\leq b})$. A value $a \in \mathbb{R}$ is a *homological critical value* of f if $\exists l \in \mathbb{Z}^*$ such that $f_l^{a-\delta,a+\delta}$ is not an isomorphism for all sufficiently small $\delta > 0$, where $\mathbb{Z}^*$ is the set of non-negative integers. We assume that f is *tame*, i.e, the number of homological critical values of f is finite and the homology groups $H_l(\mathbb{M}_{\leq a})$ are finite-dimensional $\forall l \in \mathbb{Z}^*$. Here, a is any homological critical value of f. Let $a_0 < a_1 < \ldots < a_N$ be the homological critical values of f. In this paper, we consider homology with coefficients in $\mathbb{Z}_2$, which is the group of integers modulo 2. Therefore, $H_l(\mathbb{M}_{\leq a_i})$ is a vector space for $0 \leq i \leq N$. We have the following sequence of vector spaces,

$$\emptyset = H_l(\mathbb{M}_{\leq a_0}) \to H_l(\mathbb{M}_{\leq a_1}) \to \cdots \to H_l(\mathbb{M}_{\leq a_N}) = H_l(\mathbb{M}). \quad (1)$$

where the homomorphisms $f_l^{a_i,a_{i+1}}$ are induced by the inclusions $\mathbb{M}_{\leq a_i} \subseteq \mathbb{M}_{\leq a_{i+1}}$. A homology class γ is born at a if $\gamma \in H_l(\mathbb{M}_a)$ but $\gamma \notin \text{Im } f_l^{a-\delta,a}$ for $0 < \delta \leq b - a$. Further, a class γ which is born at a dies at b if $f_l^{a,b-\delta}(\gamma) \notin \text{Im } f_l^{a-\delta,b-\delta}$ for any $\delta > 0$, but $f_l^{a,b}(\gamma) \in \text{Im } f_l^{a-\delta,b}$. Such birth and death events are recorded by persistent homology. The l-th ordinary persistence diagram is a multiset of points in $\overline{\mathbb{R}}^2$, where $\overline{\mathbb{R}} = \mathbb{R} \cup \{-\infty, +\infty\}$. Each point (a, b) in the lth ordinary persistence diagram corresponds to a l-homology class which is born at a and dies at b. The multiplicity of a point (a, b) with $a \leq b$ is defined in terms of the ranks of the homomorphism $f_l^{a,b}$ and the points along the diagonal have infinite multiplicity.

In general, not all homology classes die during the sequence in equation (1). Such homology classes are is said to be essential. An essential homology class of dimension l is denoted by a point (a_i, ∞) in the lth ordinary persistence diagram, where a_i is the critical value corresponding to the birth of the homology class. By appending a sequence of relative homology groups to equation (1), we obtain the following sequence:

$$\begin{aligned} &\emptyset = H_l(\mathbb{M}_{\leq a_0}) \to H_l(\mathbb{M}_{\leq a_1}) \to \cdots \to H_l(\mathbb{M}_{\leq a_N}) = H_l(\mathbb{M}) \\ &= H_l(\mathbb{M}, \mathbb{M}_{\geq a_N}) \to H_l(\mathbb{M}, \mathbb{M}_{\geq a_{N-1}}) \to \cdots \to H_l(\mathbb{M}, \mathbb{M}_{\geq a_0}) = \emptyset. \end{aligned} \quad (2)$$

where $\mathbb{M}_{\geq a_i}$ denotes the super-level set of f, $\mathbb{M}_{\geq a_i} = f^{-1}[a_i, \infty)$ and $H_l(\mathbb{M}, \mathbb{M}_{\geq a_i})$ is a relative homology group [15]. Essential homology classes are created in the ordinary part and are destroyed in the relative part of the sequence in equation (2). The birth and death of essential homology classes are encoded by the extended persistence diagram. An essential homology class of dimension l which is born at $H_l(\mathbb{M}_{\leq a_i})$ and dies at $H_l(\mathbb{M}, \mathbb{M}_{\geq a_j})$ is denoted by the point (a_i, a_j) in the lth extended persistence diagram.

3.4 Bottleneck Distance between Persistence Diagrams

The bottleneck distance between persistence diagrams X and Y is defined as follows:

$$d_B(X, Y) = \inf_{\eta: X \to Y} \max_{x \in X} ||\mathbf{x} - \eta(x)||_\infty \quad (3)$$

where η ranges over bijections between X and Y. For each point (a, b) in X, we add its nearest diagonal point $(\frac{a+b}{2}, \frac{a+b}{2})$ in Y and vice-versa. The number of points in X and Y are now equal. To compute the bottleneck distance, a bijection $\eta : X \to Y$ is constructed such that $\max_{x \in X} ||x - \eta(x)||_\infty$ is minimized.

3.5 Reeb Graph and Persistence Diagram

Let f be a real-valued continuous function defined on $\mathbb{M}$. The Reeb graph of f, denoted by $\mathcal{RG}_f$, is the quotient space of contours of f. The function f induces a real-valued function $\bar{f} : \mathcal{RG}_f \to \mathbb{R}$, which takes each point in $p \in \mathcal{RG}_f$ to the value of f corresponding to its contour $\tilde{f}^{-1}(p)$ in the domain, $f = \bar{f} \circ \tilde{f}$.

The persistence of topological features of $\mathcal{RG}_f$ are encoded in the persistence diagrams $\mathrm{Dg}_0(\mathcal{RG}_f)$, $\mathrm{Dg}_0(\mathcal{RG}_{-f})$, $\mathrm{ExDg}_0(\mathcal{RG}_f)$ and $\mathrm{ExDg}_1(\mathcal{RG}_f)$. The 0-dimensional persistent homological features corresponding to the sub-level set and super-level set filtrations of f are captured in $\mathrm{Dg}_0(\mathcal{RG}_f)$ and $\mathrm{Dg}_0(\mathcal{RG}_{-f})$ respectively. $\mathrm{ExDg}_0(\mathcal{RG}_f)$ encodes the range of f and $\mathrm{ExDg}_1(\mathcal{RG}_f)$ captures the 1-cycles or loops in $\mathcal{RG}_f$.

To compute the persistence diagrams of $\mathcal{RG}_f$, we require $\mathcal{RG}_f$ to be the Reeb graph of a Morse function. If f is a *Morse function*, i.e. all its critical points are non-degenerate and are at different levels, then the critical nodes of $\mathcal{RG}_f$ have distinct values of $\bar{f}$ and belong to one of the following five-types: (i) a minimum (with down-degree = 0, up-degree = 1), (ii) a maximum (with up-degree = 0, down-degree = 1), (iii) a down-fork (with down-degree = 2, up-degree = 1) and (iv) a up-fork (with up-degree = 2, down-degree = 1). A regular node has up-degree = 1 and down-degree = 1. A down-fork (similarly, up-fork) node is called an essential down-fork node when it contributes to a loop (cycle) of the Reeb graph. Otherwise it is called an ordinary down-fork node. To ensure that $\mathcal{RG}_f$ is the Reeb graph of a Morse function, we first eliminate degenerate critical nodes in $\mathcal{RG}_f$ by breaking them into non-degenerate critical nodes [38]. After eliminating degenerate critical nodes, we ensure that the critical nodes of $\bar{f}$ are at different levels. If two critical nodes are at the same level, then the value of one of the nodes is increased/decreased by a small value ϵ. After removing degenerate critical nodes and ensuring that critical nodes are at different levels, $\mathcal{RG}_f$ becomes the Reeb graph of a Morse function.

The points in $\mathrm{Dg}_0(f)$ are computed by pairing ordinary down-forks with minima, ordinary up-forks with maxima and the global minimum with global maximum. Let u be an ordinary down-fork of $\mathcal{RG}_f$. The two lower branches of u correspond to two different components C_1 and C_2 in $(\mathcal{RG}_f)_{\leq \bar{f}(u)}$. Let x_1 and x_2 be the global minimum of C_1 and C_2 respectively. Let us assume that $\bar{f}(x_1) < \bar{f}(x_2)$. Then a 0-dimensional homology class is born at x_2 and dies at u. x_2 is paired with u and point $(\bar{f}(x_2), \bar{f}(u))$ is created in $\mathrm{Dg}_0(\mathcal{RG}_f)$ (see Figure 2(b)). A symmetric procedure is applied on $\mathcal{RG}_{-f}$ to obtain points in $\mathrm{Dg}_0(\mathcal{RG}_{-f})$ by pairing up-forks with maxima. Let $x, y \in \mathcal{RG}_f$ correspond to the global minimum and maximum of $\bar{f}$ respectively. We pair x with y, giving rise to the point $(\bar{f}(x), \bar{f}(y))$ in $\mathrm{ExDg}_0(\mathcal{RG}_f)$ (see Figure 2(c)).

We are interested in the persistent features which are born and die within the range of $\bar{f}$. In Figure 2(b), the point $(1, \infty) \in \mathrm{Dg}_0(\mathcal{RG}_f)$ corresponds to the unique homology class born at the global minimum of f and persists throughout the sub-level set filtration. However, the point $(1, 12) \in \mathrm{ExDg}_0(\mathcal{RG}_f)$ encodes both the minimum and maximum of $\bar{f}$ (see Figure 2(c)). Therefore, $\mathrm{Dg}_0(\mathcal{RG}_f)$ is combined with $\mathrm{ExDg}_0(\mathcal{RG}_f)$ to obtain $\mathrm{PD}_0(\mathcal{RG}_f)$. This persistence diagram consists of the points in $\mathrm{Dg}_0(\mathcal{RG}_f)$ except the point with infinite persistence $(1, \infty)$, instead the point $(1, 12)$ in $\mathrm{ExDg}_0(\mathcal{RG}_f)$ is included. Thus $\mathrm{PD}_0(\mathcal{RG}_f) := \mathrm{Dg}_0(\mathcal{RG}_f) \cup \mathrm{ExDg}_0(\mathcal{RG}_f) \setminus \{(1, \infty)\}$ (see Figure 2(d)).

To compute the points in the 1st extended persistence diagram $\mathrm{ExDg}_1(\mathcal{RG}_f)$, we pair essential down-forks with essential up-forks. Let u be an essential down-fork of $\mathcal{RG}_f$. Of all the cycles born at u, let γ be a cycle having the largest minimum value of $\bar{f}$. Let $v \in \gamma$ be the node corresponding to the minimum on γ. It can be seen

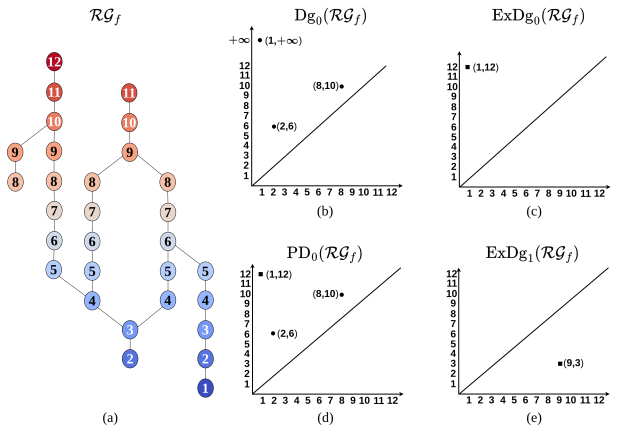

Figure 2: (a) Reeb graph of a scalar field f. (b) 0th ordinary persistence diagram $\mathrm{Dg}_0(\mathcal{RG}_f)$. (c) 0th extended persistence diagram $\mathrm{ExDg}_0(\mathcal{RG}_f)$. (d) $\mathrm{PD}_0(\mathcal{RG}_f) := \mathrm{Dg}_0(\mathcal{RG}_f) \cup \mathrm{ExDg}_0(\mathcal{RG}_f) \setminus \{(1, \infty)\}$. (e) 1st extended persistence diagram $\mathrm{ExDg}_1(\mathcal{RG}_f)$. The points in ordinary (extended) persistence diagrams are denoted by circular points (squares).

that v is an essential up-fork [1]. u is paired with v giving rise to the point $(\bar{f}(u), \bar{f}(v))$ in $\mathrm{ExDg}_1(f)$ (see Figure 2(e)). In this paper, we compute the persistence diagrams PD_0 and ExDg_1 of the Reeb graphs in an MDRG.

3.6 Laplace Beltrami Operator

Let $\mathcal{M}$ be a Riemannian 2-manifold in $\mathbb{R}^3$. For a twice-differentiable function $f : \mathcal{M} \to \mathbb{R}$, the Laplace Beltrami (LB) operator $\Delta_{\mathcal{M}}$ is defined as follows:

$$\Delta_{\mathcal{M}} f = div(grad\ f) \tag{4}$$

where grad f is the gradient of f and div is the divergence on the manifold [9]. Let ψ be a diffeormorphism from an open set $U \subset \mathcal{M}$ to $\mathbb{R}^2$ with

$$g_{ij} = \langle \partial_i \psi, \partial_j \psi \rangle, G = (g_{ij}),$$
$$W = \sqrt{|G|}, (g^{ij}) = G^{-1},$$

where the matrix G is a *Riemannian tensor* on $\mathcal{M}$ and $|G|$ is the determinant of G. The LB operator can now be written as follows [28]:

$$\Delta_{\mathcal{M}} f = \frac{1}{W} \sum_{i,j=1}^{2} \partial_i (g^{ij} W \partial_j f). \tag{5}$$

The Riemannian metric g determines the intrinsic properties of $\mathcal{M}$, which are independent of the embedding of $\mathcal{M}$. Further, since the definition of g is based on inner products which are rotation invariant, g is also invariant to rotations of $\mathcal{M}$.

3.6.1 Discretization of the Laplace Beltrami operator. Let $\mathbb{M}$ be a triangulation of the surface $\mathcal{M}$, with $\mathcal{V} = \{v_1, v_2, ..., v_n\}$ as the set of vertices. Two vertices in $\mathbb{M}$ are said to be adjacent if they are connected by an edge. The set of adjacent vertices of v_i is denoted

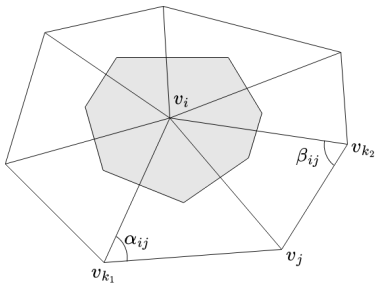

Figure 3: Definition of the angles α_{ij} and β_{ij} and the area of the Voronoi cell (shaded region) corresponding to vertex v_i.

by $N(v_i)$. The LB operator at a vertex v_i is written as follows:

$$\Delta_{\mathbb{M}} = \frac{1}{s_i} \sum_{v_j \in N(v_i)} \frac{\cot \alpha_{ij} + \cot \beta_{ij}}{2} [f(v_j) - f(v_i)]. \tag{6}$$

where, s_i is the area of the Voronoi cell (shaded region) shown in Figure 3.

A weight function is defined as follows:

$$m_{ij} = \begin{cases} \frac{\cot \alpha_{ij} + \cot \beta_{ij}}{2} & \text{if } v_i \text{ and } v_j \text{ are adjacent} \\ 0 & \text{otherwise.} \end{cases} \tag{7}$$

When f is restricted to the vertices of $\mathbb{M}$, its discrete version is $\vec{f}$ with $f_i = f(v_i)$. The discrete LB operator of f is written as $\Delta_{\mathbb{M}} f \approx L\vec{f}$. The entries of the matrix L are given by

$$L_{ij} = \begin{cases} \sum_k \frac{m_{ik}}{s_i} \text{ if } i = j, \\ -\frac{m_{ij}}{s_i} \text{ if } v_i \text{ and } v_j \text{ are adjacent,} \\ 0 \text{ otherwise.} \end{cases}$$

The eigenvalues and eigenfunctions of the discrete version of the LB operator are computed by solving the eigenvalue problem $L\vec{v} = \lambda\vec{v}$. We note, the matrix L is not symmetric since s_i need not be the same for all vertices of $\mathbb{M}$. Therefore, the set of eigenvalues of this problem is not guaranteed to be real [30]. However, the matrix L can be factorized as $L = S^{-1}M$, where S is a diagonal matrix with $S_{ii} = s_i$ and M is defined as follows:

$$M_{ij} = \begin{cases} \sum_i m_{ij} \text{ if } i = j, \\ -m_{ij} \text{ if } v_i \text{ and } v_j \text{ are adjacent,} \\ 0 \text{ otherwise.} \end{cases} \tag{8}$$

The eigenvalue problem $L\vec{v} = \lambda\vec{v}$ is rewritten as the generalized eigenvalue problem $S^{-1}M\vec{v} = \lambda\vec{v}$, or

$$M\vec{v} = \lambda S\vec{v}. \tag{9}$$

Since the matrices S and M are symmetric and S is positive-definite, the eigenvalues and eigenvectors are real. Further, the eigenvalues are non-negative and the eigenvectors are orthogonal in terms of S-inner product:

$$\langle \vec{u}, \vec{v} \rangle_S = \vec{u}^T S\vec{v}.$$

In this paper, we obtain the feature descriptors of a shapes based on the eigenfunctions of LB operator.

4 PROPOSED DISTANCE BETWEEN MDRGS

In this section, we propose a distance measure between shapes by defining a distance measure between two MDRGs based on the bottleneck distance between Reeb graphs [4]. First we discuss our measure for bivariate fields.

4.1 Distance between bivariate fields

Let $\mathbf{f} = (f_1, f_2), \mathbf{g} = (g_1, g_2)$ be two piecewise linear bivariate fields defined on $\mathbb{M}$ and let $\mathbb{MR}_{\mathbf{f}}$ and $\mathbb{MR}_{\mathbf{g}}$ be the corresponding MDRGs. To compute the proposed distance between $\mathbb{MR}_{\mathbf{f}}$ and $\mathbb{MR}_{\mathbf{g}}$, we compute a sum of bottleneck distances between the component Reeb graphs in each dimension of the MDRGs by considering all possible bijections between the component Reeb graphs.

In the first dimension of the MDRGs, there is only one Reeb graph corresponding to each of the fields f_1 and g_1, denoted by $\mathcal{RG}_{f_1}$ and $\mathcal{RG}_{g_1}$, respectively. Let, $Range(f_1) = [\min_{x \in \mathbb{M}} f_1(x), \max_{x \in \mathbb{M}} f_1(x)]$ and $Range(g_1) = [\min_{x \in \mathbb{M}} g_1(x), \max_{x \in \mathbb{M}} g_1(x)]$ be the ranges of the functions f_1 and g_1. We define $R(f_1, g_1) = Range(f_1) \cup Range(g_1)$ as the union of the ranges of f_1 and g_1. Now for each $c \in R(f_1, g_1)$, in the second dimension, the MDRGs $\mathbb{MR}_{\mathbf{f}}$ and $\mathbb{MR}_{\mathbf{g}}$ may have multiple Reeb graphs corresponding to f_2 and g_2 restricted on $f_1^{-1}(c)$ and $g_1^{-1}(c)$, respectively. Let $\mathbb{S}^c_{f_1} = \{\mathcal{RG}_{\widetilde{f_2^p}} | \tilde{f}_1(p) = c\}$ be the set of Reeb graphs from the second dimension of $\mathbb{MR}_{\mathbf{f}}$ and $\mathbb{S}^c_{g_1} = \{\mathcal{RG}_{\widetilde{g_2^p}} | \tilde{g}_1(p) = c\}$ be the set of Reeb graphs from the second dimension of $\mathbb{MR}_{\mathbf{g}}$. We consider all possible bijections ψ_c between $\mathbb{S}^c_{f_1}$ and $\mathbb{S}^c_{g_1}$. Since the number of Reeb graphs in $\mathbb{S}^c_{f_1}$ and $\mathbb{S}^c_{g_1}$ need not be equal, it may not be possible to construct proper bijections between $\mathbb{S}^c_{f_1}$ and $\mathbb{S}^c_{g_1}$. Therefore, to construct ψ_c we introduce dummy Reeb graphs (without vertices and edges) in $\mathbb{S}^c_{f_1}$ or $\mathbb{S}^c_{g_1}$ to make the cardinality of $\mathbb{S}^c_{f_1}$ and $\mathbb{S}^c_{g_1}$ equal.

We now define a distance between $\mathbb{MR}_{\mathbf{f}}$ and $\mathbb{MR}_{\mathbf{g}}$ as follows.

$$d_{\mathbb{MR}}\left(\mathbb{MR}_{\mathbf{f}}, \mathbb{MR}_{\mathbf{g}}\right) = d_B\left(\mathrm{Dg}\left(\mathcal{RG}_{f_1}\right), \mathrm{Dg}\left(\mathcal{RG}_{g_1}\right)\right) + \frac{1}{|R(f_1, g_1)|} \int_{c \in R(f_1, g_1)} \inf_{\psi_c : \mathbb{S}^c_{f_1} \to \mathbb{S}^c_{g_1}} \sup_{\mathcal{RG} \in \mathbb{S}^c_{f_1}} d_B\left(\mathrm{Dg}\left(\mathcal{RG}\right), \mathrm{Dg}\left(\psi_c\left(\mathcal{RG}\right)\right)\right) \tag{10}$$

where $\mathrm{Dg}(\mathcal{RG})$ is a persistence diagram of the Reeb graph $\mathcal{RG}$, ψ_c ranges over bijections between $\mathbb{S}^c_{f_1}$ and $\mathbb{S}^c_{g_1}$. If $Range(f_1) \cap Range(g_1) \neq \emptyset$, then $|R(f_1, g_1)|$ is the length of the interval $R(f_1, g_1)$, otherwise $|R(f_1, g_1)| = |Range(f_1)| + |Range(g_1)|$. Here, we note, ψ_c can map a Reeb graph in $\mathbb{S}^c_{f_1}$ to a dummy Reeb graph. The persistence diagram corresponding to a dummy Reeb graph is empty, i.e, it does not contain any point. The bottleneck distance between persistence diagrams is computed as described in section 3.4.

In the current paper, corresponding to each of the Reeb graph in an MDRG, we construct two persistence diagrams, namely PD_0 and ExDg_1, as discussed in section 3.5. We compute the distance between MDRGs defined in equation (10) based on PD_0 and ExDg_1, which are denoted by $d^0_{\mathbb{MR}}(\mathbb{MR}_{\mathbf{f}}, \mathbb{MR}_{\mathbf{g}})$ and $d^1_{\mathbb{MR}}(\mathbb{MR}_{\mathbf{f}}, \mathbb{MR}_{\mathbf{g}})$, respectively. We consider the proposed distance measure between $\mathbb{MR}_{\mathbf{f}}$ and $\mathbb{MR}_{\mathbf{g}}$ as the weighted sum of $d^0_{\mathbb{MR}}\left(\mathbb{MR}_{\mathbf{f}}, \mathbb{MR}_{\mathbf{g}}\right)$,

$d^0_{\mathbb{MR}}\left(\mathbb{MR}_{-\mathbf{f}}, \mathbb{MR}_{-\mathbf{g}}\right)$ and $d^1_{\mathbb{MR}}\left(\mathbb{MR}_{\mathbf{f}}, \mathbb{MR}_{\mathbf{g}}\right)$.

$$d_T(\mathbb{MR}_{\mathbf{f}}, \mathbb{MR}_{\mathbf{g}}) = w_0 \cdot d^0_{\mathbb{MR}}\left(\mathbb{MR}_{\mathbf{f}}, \mathbb{MR}_{\mathbf{g}}\right) + w_1 \cdot d^0_{\mathbb{MR}}\left(\mathbb{MR}_{-\mathbf{f}}, \mathbb{MR}_{-\mathbf{g}}\right) + w_2 \cdot d^1_{\mathbb{MR}}\left(\mathbb{MR}_{\mathbf{f}}, \mathbb{MR}_{\mathbf{g}}\right) \quad (11)$$

where, $0 \leq w_0, w_1, w_2 \leq 1$ and $w_0 + w_1 + w_2 = 1$. Here, $d^0_{\mathbb{MR}}\left(\mathbb{MR}_{\mathbf{f}}, \mathbb{MR}_{\mathbf{g}}\right)$ and $d^0_{\mathbb{MR}}\left(\mathbb{MR}_{-\mathbf{f}}, \mathbb{MR}_{-\mathbf{g}}\right)$ respectively compute the distance between persistence diagrams of sub-level set and super and level set filtrations of the Reeb graphs in the MDRGs and $d^1_{\mathbb{MR}}\left(\mathbb{MR}_{\mathbf{f}}, \mathbb{MR}_{\mathbf{g}}\right)$ is the distance between the 1-st extended persistence diagrams of the Reeb graphs in $\mathbb{MR}_{\mathbf{f}}$ and $\mathbb{MR}_{\mathbf{g}}$ respectively. The following theorem shows that the d_T is a pseudo-metric.

Theorem 4.1. *d_T satisfies the properties of a pseudo-metric.*

Proof. **Non-negativity:** For two MDRGs $\mathbb{MR}_{\mathbf{f}}$ and $\mathbb{MR}_{\mathbf{g}}$, we have $d_T(\mathbb{MR}_{\mathbf{f}}, \mathbb{MR}_{\mathbf{g}}) \geq 0$. Thus the non-negativity property is satisfied.

Symmetry: For two MDRGs $\mathbb{MR}_{\mathbf{f}}$ and $\mathbb{MR}_{\mathbf{g}}$, we have $d_T(\mathbb{MR}_{\mathbf{f}}, \mathbb{MR}_{\mathbf{g}}) = d_T(\mathbb{MR}_{\mathbf{g}}, \mathbb{MR}_{\mathbf{f}})$. Thus the symmetry property holds.

Identity: Bauer *et al*. [4] showed that two distinct Reeb graphs can have the same persistence diagram and therefore the bottleneck distance between Reeb graphs is a pseudo-metric. Since we compute $d_T(\mathbb{MR}_{\mathbf{f}}, \mathbb{MR}_{\mathbf{g}})$ by calculating the bottleneck distance between the component Reeb graphs of the MDRGs $\mathbb{MR}_{\mathbf{f}}$ and $\mathbb{MR}_{\mathbf{g}}$, it follows that the bottleneck distance between two non-identical MDRGs $\mathbb{MR}_{\mathbf{f}}$ and $\mathbb{MR}_{\mathbf{g}}$ can be zero. Therefore, the identity property does not hold.

Triangle inequality: Let us consider three MDRGs $\mathbb{MR}_{\mathbf{f}}, \mathbb{MR}_{\mathbf{g}}$ and $\mathbb{MR}_{\mathbf{h}}$, corresponding to bivariate fields $\mathbf{f} = (f_1, f_2)$, $\mathbf{g} = (g_1, g_2)$ and $\mathbf{h} = (h_1, h_2)$, respectively. We first prove the triangle inequality property for $d^0_{\mathbb{MR}}$ between MDRGs. We need to show that $d^0_{\mathbb{MR}}(\mathbb{MR}_{\mathbf{f}}, \mathbb{MR}_{\mathbf{h}}) \leq d^0_{\mathbb{MR}}(\mathbb{MR}_{\mathbf{f}}, \mathbb{MR}_{\mathbf{g}}) + d^0_{\mathbb{MR}}(\mathbb{MR}_{\mathbf{g}}, \mathbb{MR}_{\mathbf{h}})$.
For $c \in R(f_1, g_1)$, let ψ'_c be the bijection between $\mathbb{S}^c_{f_1}$ and $\mathbb{S}^c_{g_1}$ achieving $d^0_{\mathbb{MR}}(\mathbb{MR}_{\mathbf{f}}, \mathbb{MR}_{\mathbf{g}})$. Similarly, let ψ''_c be the bijection between $\mathbb{S}^c_{g_1}$ and $\mathbb{S}^c_{h_1}$ achieving $d^0_{\mathbb{MR}}(\mathbb{MR}_{\mathbf{g}}, \mathbb{MR}_{\mathbf{h}})$. Let ψ'''_c be the bijection between $\mathbb{S}^c_{f_1}$ and $\mathbb{S}^c_{h_1}$ obtained by the composition of ψ''_c and ψ'_c, i.e, $\psi'''_c = \psi''_c \circ \psi'_c$.

$$\begin{aligned}
&d^0_{\mathbb{MR}}\left(\mathbb{MR}_{\mathbf{f}}, \mathbb{MR}_{\mathbf{h}}\right) \\
&= d_B\left(\mathrm{PD}_0\left(\mathcal{RG}_{f_1}\right), \mathrm{PD}_0\left(\mathcal{RG}_{h_1}\right)\right) + \\
&\frac{1}{|R(f_1,h_1)|} \int_{c \in R(f_1,h_1)} \inf_{\psi_c : \mathbb{S}^c_{f_1} \to \mathbb{S}^c_{h_1}} \sup_{\mathcal{RG} \in \mathbb{S}^c_{f_1}} d_B\left(\mathrm{PD}_0\left(\mathcal{RG}\right), \mathrm{PD}_0\left(\psi_c\left(\mathcal{RG}\right)\right)\right) \\
&\leq d_B\left(\mathrm{PD}_0\left(\mathcal{RG}_{f_1}\right), \mathrm{PD}_0\left(\mathcal{RG}_{h_1}\right)\right) + \\
&\quad \frac{1}{|R(f_1,h_1)|} \int_{c \in R(f_1,h_1)} \sup_{\mathcal{RG} \in \mathbb{S}^c_{f_1}} d_B\left(\mathrm{PD}_0\left(\mathcal{RG}\right), \mathrm{PD}_0\left(\psi'''_c\left(\mathcal{RG}\right)\right)\right) \\
&\leq d^0_{\mathbb{MR}}(\mathbb{MR}_{\mathbf{f}}, \mathbb{MR}_{\mathbf{g}}) + d^0_{\mathbb{MR}}(\mathbb{MR}_{\mathbf{g}}, \mathbb{MR}_{\mathbf{h}}) \\
&\qquad \text{(since } d_B \text{ between Reeb graphs is a pseudo-metric).}
\end{aligned}$$

Using a similar argument, we can prove the triangle inequality for $d^1_{\mathbb{MR}}$. We now show the triangle inequality property for $d_T(\mathbb{MR}_{\mathbf{f}}, \mathbb{MR}_{\mathbf{h}})$.

$$\begin{aligned}
&d_T(\mathbb{MR}_{\mathbf{f}}, \mathbb{MR}_{\mathbf{h}}) \\
&= w_0 \cdot d^0_{\mathbb{MR}}\left(\mathbb{MR}_{\mathbf{f}}, \mathbb{MR}_{\mathbf{h}}\right) + w_1 \cdot d^0_{\mathbb{MR}}\left(\mathbb{MR}_{-\mathbf{f}}, \mathbb{MR}_{-\mathbf{h}}\right) \\
&\quad + w_2 \cdot d^1_{\mathbb{MR}}\left(\mathbb{MR}_{\mathbf{f}}, \mathbb{MR}_{\mathbf{h}}\right) \\
&\leq w_0 \left(d^0_{\mathbb{MR}}\left(\mathbb{MR}_{\mathbf{f}}, \mathbb{MR}_{\mathbf{g}}\right) + d^0_{\mathbb{MR}}\left(\mathbb{MR}_{\mathbf{g}}, \mathbb{MR}_{\mathbf{h}}\right)\right) + \\
&\quad w_1 \left(d^0_{\mathbb{MR}}\left(\mathbb{MR}_{-\mathbf{f}}, \mathbb{MR}_{-\mathbf{g}}\right) + d^0_{\mathbb{MR}}\left(\mathbb{MR}_{-\mathbf{g}}, \mathbb{MR}_{-\mathbf{h}}\right)\right) + \\
&\quad w_2 \left(d^1_{\mathbb{MR}}\left(\mathbb{MR}_{\mathbf{f}}, \mathbb{MR}_{\mathbf{g}}\right) + d^1_{\mathbb{MR}}\left(\mathbb{MR}_{\mathbf{g}}, \mathbb{MR}_{\mathbf{h}}\right)\right) \\
&= w_0 \cdot d^0_{\mathbb{MR}}\left(\mathbb{MR}_{\mathbf{f}}, \mathbb{MR}_{\mathbf{g}}\right) + w_1 \cdot d^0_{\mathbb{MR}}\left(\mathbb{MR}_{-\mathbf{f}}, \mathbb{MR}_{-\mathbf{g}}\right) \\
&\quad + w_2 \cdot d^1_{\mathbb{MR}}\left(\mathbb{MR}_{\mathbf{f}}, \mathbb{MR}_{\mathbf{g}}\right) + w_0 \cdot d^0_{\mathbb{MR}}\left(\mathbb{MR}_{\mathbf{g}}, \mathbb{MR}_{\mathbf{h}}\right) \\
&\quad + w_1 \cdot d^0_{\mathbb{MR}}\left(\mathbb{MR}_{-\mathbf{g}}, \mathbb{MR}_{-\mathbf{h}}\right) + w_2 \cdot d^1_{\mathbb{MR}}\left(\mathbb{MR}_{\mathbf{g}}, \mathbb{MR}_{\mathbf{h}}\right) \\
&= d_T(\mathbb{MR}_{\mathbf{f}}, \mathbb{MR}_{\mathbf{g}}) + d_T(\mathbb{MR}_{\mathbf{g}}, \mathbb{MR}_{\mathbf{h}}).
\end{aligned}$$

□

The proposed measure d_T also satisfies the *stability* property which is proved in Appendix A.

4.2 Generalization for more than two fields

Although, in this paper, we deal with MDRGs of bivariate fields and persistence diagrams of dimensions 0 and 1, the proposed distance measure can be extended for MDRGs corresponding to more than 2 fields and for any k-dimensional persistence diagrams. If $\mathbf{f} = (f_1, f_2, .., f_r) : \mathbb{M} \to \mathbb{R}^r$ and $\mathbf{g} = (g_1, g_2, ..., g_r) : \mathbb{M} \to \mathbb{R}^r$ are multi-fields defined on a triangulated mesh $\mathbb{M}$ of dimension $d \geq r$, then the distance between the MDRGs $\mathbb{MR}_{\mathbf{f}}$ and $\mathbb{MR}_{\mathbf{g}}$ based on their k-th ordinary persistence diagrams Dg_k is defined as follows:

$$\begin{aligned}
&d^k_{\mathbb{MR}}\left(\mathbb{MR}_{\mathbf{f}}, \mathbb{MR}_{\mathbf{g}}\right) = d_B\left(\mathrm{Dg}_k\left(\mathcal{RG}_{f_1}\right), \mathrm{Dg}_k\left(\mathcal{RG}_{g_1}\right)\right) + \\
&\sum_{i=1}^{r-1} \frac{1}{|R(f_i,g_i)|} \int_{c \in R(f_i,g_i)} \inf_{\psi^{(i)}_c : \mathbb{S}^c_{f_i} \to \mathbb{S}^c_{g_i}} \sup_{\mathcal{RG} \in \mathbb{S}^c_{f_i}} d_B\left(\mathrm{Dg}_k(\mathcal{RG}), \mathrm{Dg}_k(\psi_i(\mathcal{RG}))\right).
\end{aligned} \quad (12)$$

Here, $\mathbb{S}^c_{f_i}$ and $\mathbb{S}^c_{g_i}$ denote the collections of Reeb graphs in the $(i+1)^{th}$ dimension of $\mathbb{MR}_{\mathbf{f}}$ and $\mathbb{MR}_{\mathbf{g}}$ respectively, $\psi^{(i)}_c$ varies over bijections between $\mathbb{S}^c_{f_i}$ and $\mathbb{S}^c_{g_i}$, and $R(f_i, g_i)$ represents the union of the ranges of f_i and g_i.

Next we discuss the feature descriptors corresponding to a shape for computing the MDRGs.

4.3 Feature Descriptors of a Shape

We obtain scalar fields based on the eigenfunctions of discrete Laplace-Beltrami operator (see equation (9)) for computing the MDRG. The eigenvalues λ_is of the discrete LB operator are sorted in the non-decreasing order. The first eigenvalue λ_0 is zero and the corresponding eigenfunctions are constant [26]. Therefore, we consider the eigenvalues λ_i for $i > 0$. The ability of the eigenfunctions in capturing the geometric and topological properties of a shape and their invariance to isometry of shapes [20, 30] make them suitable shape descriptors.

To remove the effect of scale, each eigenfunction is normalized by its corresponding eigenvalue [30]. For a triangulated shape with vertices $v_1, v_2, ..., v_n$, the normalized eigenfunction corresponding to eigenvalue λ_i is an n-dimensional vector $\hat{\phi}_i = \left(\frac{\phi_i(v_1)}{\sqrt{\lambda_i}}, \frac{\phi_i(v_2)}{\sqrt{\lambda_i}}, ..., \frac{\phi_i(v_n)}{\sqrt{\lambda_i}}\right)$, where $\phi_i(v_j)$ is the value of the i^{th} eigenfunction at the vertex v_j.

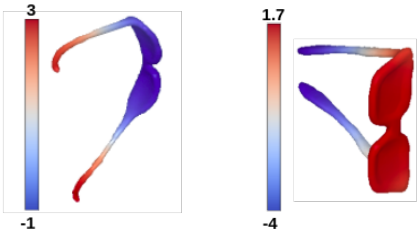

Figure 4: Eigenfunction ϕ_3 of similar shapes.

4.3.1 Sign Ambiguity Problem. We now encounter the sign ambiguity problem while dealing with the eigenfunctions of the LB operator. If ϕ_i is an eigenfunction corresponding to the eigenvalue λ_i , then $-\phi_i$ is also an eigenfunction for λ_i. We have to pick one among them as the eigenfunction for λ_i. If we arbitrarily choose either of ϕ_i or $-\phi_i$, then there is a possibility of two similar shapes having eigenfunctions which are negative of each other (See Figure 4). Therefore, for each eigenvalue λ_i, we need to systematically pick one of ϕ_i or $-\phi_i$. This is known as the sign ambiguity problem [23], for which Umeyama *et al*. [39] proposed a solution by taking the absolute of eigenfunctions. In this paper, we adopt this solution and choose the functions $\left|\hat{\phi}_i\right|$ as shape descriptors.

5 EXPERIMENTAL RESULTS

In this section, we show the experimental results of the proposed measure in matching shapes and compare the results with various topological distance measures in the literature. We show the effectiveness of using eigenfunctions as feature descriptors with respect to HKS [36], WKS [3] and SIHKS [5].

The descriptors HKS and SIHKS depend on the number of time parameters [5, 36] and WKS depends on the number of energy distributions [3]. Following [21], we have fixed the number of time parameters as 10 for HKS, 17 for SIHKS, and the number of energy distributions as 10 for WKS. The number of eigenfunctions is chosen as 200 for constructing HKS, WKS and SIHKS. The distance between two shapes with respect to a distance measure d is defined as the sum of distances computed at each time (for HKS, SIHKS) or energy distribution (for WKS). For example, the distance between shapes S_1 and S_2 using HKS is given by:

$$d_{HKS} = \sum_{t=1}^{10} d(h_t(S_1), h_t(S_2)) \tag{13}$$

where d is the distance measure and h_t is the HKS at time t.

5.1 SHREC 2010 Dataset

The Shape Retrieval Contest (SHREC) 2010 dataset [22] consists of 200 watertight shapes classified into 10 categories. A sample of the shapes are shown in Figure 5. Each of the meshes is simplified into 2000 faces [21]. We compare the performance of the proposed distance between MDRGs with the distance between MRSs [25] and the distance between histograms corresponding to fiber-component distributions [2]. We evaluate the efficiency of distance measures by the standard evaluation techniques NN, FT, ST, E-measure, and DCG (see [22] for details). These techniques take a distance matrix

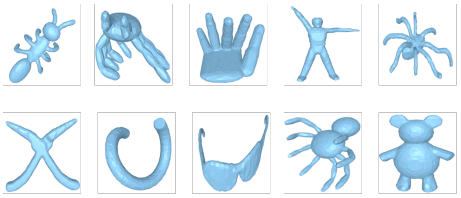

Figure 5: Collection of shapes from SHREC 2010.

consisting of distances between all pairs of shapes and return a value between 0 and 1, where higher values indicate better efficiency.

We first show the significance of bivariate fields over scalar fields using the proposed distance measure d_T. Table 1 shows the results of d_T between MDRGs using a pair of eigenfunctions (bivariate field) and the bottleneck distance between Reeb graphs using individual eigenfunctions (scalar field). The bivariate field using MDRG produces a better result than the Reeb graphs of the individual scalar fields, thereby indicating its significance.

Descriptor	NN	1-Tier	2-Tier	e-Measure	DCG
$\left\|\hat{\phi}_1\right\|$	0.8100	0.5461	0.6950	0.4963	0.8172
$\left\|\hat{\phi}_2\right\|$	0.7800	0.4437	0.5924	0.4131	0.7764
$\left(\left\|\hat{\phi}_1\right\|, \left\|\hat{\phi}_2\right\|\right)$	0.8600	0.5784	0.7187	0.5159	0.8412

Table 1: Performance Results. Comparison of the proposed distance between MDRGs for the bivariate field $\left(\left|\hat{\phi}_1\right|, \left|\hat{\phi}_2\right|\right)$ with the bottleneck distance between Reeb graphs corresponding to the scalar fields $\left|\hat{\phi}_1\right|$ and $\left|\hat{\phi}_2\right|$, respectively.

The efficiency in computing the distance between shapes will be higher when the shapes are compared based on many eigenfunctions. However, a 3D shape is a 2-dimensional manifold. If more than 2 fields are applied on a shape, then the corresponding Reeb space is not defined. Therefore, we generalize the distance between shapes S_1 and S_2 for more than two eigenfunctions as follows.

$$d(S_1, S_2) = \sum_{i=1}^{E-1} d_T\left(\mathbb{MR}_{\left|\hat{\phi}_i\right|,\left|\hat{\phi}_{i+1}\right|}(S_1), \mathbb{MR}_{\left|\hat{\phi}_i\right|,\left|\hat{\phi}_{i+1}\right|}(S_2)\right) \tag{14}$$

where E is the number of eigenfunctions and $\mathbb{MR}_{\left|\hat{\phi}_i\right|,\left|\hat{\phi}_{i+1}\right|}(S_k)$ is the MDRG for the shape S_k with $\left|\hat{\phi}_i\right|$ and $\left|\hat{\phi}_{i+1}\right|$ as the component scalar fields. Table 2 shows the performance of the proposed method for varying number of eigenfunctions. The results clearly indicate the increase in efficiency with increase in the number of eigenfunctions.

N	NN	1-Tier	2-Tier	e-Measure	DCG
2	0.8600	0.5784	0.7187	0.5159	0.8412
4	0.9200	0.6318	0.7576	0.5435	0.8700
6	0.9450	0.6729	0.8058	0.5735	0.8920
8	0.9450	0.7000	0.8416	0.5963	0.9127
10	0.9650	0.7518	0.8695	0.6263	0.9367
12	0.9650	0.7587	0.8734	0.6308	0.9410

Table 2: Performance of the proposed distance between MDRGs for varying number of eigenfunctions.

Table 3 shows the performance of HKS, WKS, SIHKS and absolute of eigenfunctions as shape descriptors for various distance measures. The distance measures for HKS, WKS and SIHKS are computed using equation (13). We set the parameters for various distance measures as follows. The distance between MDRGs is computed as specified in equation (14), where $E = 12$ and the weights w_0, w_1 and w_2 are set equally. The number of slabs for constructing the JCNs (required for computing MDRGs) is 32 , the parameters w and q for the distance between fiber-component distributions are set to 1 and the MRSs are constructed for 6 resolutions.

Descriptors	Methods	NN	1-Tier	2-Tier	e-Measure	DCG
HKS	Histogram	0.9200	0.5084	0.6537	0.4588	0.8200
	MRS	0.9250	0.6821	0.8211	0.5965	0.9001
	PD of Reeb graph	0.9600	0.5805	0.7208	0.5112	0.8695
WKS	Histogram	0.9400	0.5008	0.6453	0.4541	0.8250
	MRS	0.9350	0.5105	0.6468	0.4604	0.8273
	PD of Reeb graph	0.8950	0.4124	0.5234	0.3731	0.7665
SIHKS	Histogram	0.9600	0.7534	0.9008	0.6522	0.9380
	MRS	0.9600	0.7576	0.8808	0.6412	0.9354
	PD of Reeb graph	0.9750	0.8258	0.9605	0.6935	0.9618
Pairs of Eigenfunctions	Histogram	0.8900	0.6153	0.7697	0.5469	0.8692
	MRS	0.9700	0.7774	0.8821	0.6431	0.9438
	PDs of MDRG	0.9650	0.7587	0.8734	0.6308	0.9410

Table 3: Performance Results for SHREC 2010 dataset. Comparison of distance measures based on fiber-component distributions [2], MRSs [25], persistence diagrams (PDs) of Reeb graphs [4] and PDs of MDRGs using the descriptors HKS, WKS, SIHKS and pairs of eigenfunctions.

From the table, it can be seen that MDRG using eigenfunctions produces better results than HKS and WKS (for all the methods). With eigenfunctions as shape descriptor, the proposed method performs better than the histogram of fiber-component distributions and the results are comparable with that of MRS. On the other hand, the bottleneck distance between Reeb graphs outperforms other methods using SIHKS. However, the proposed measure using eigenfunctions performs better than the bottleneck distance between Reeb graphs using SIHKS when we experiment with 7 categories of shapes, which can be observed in the distance matrices in Figure 7.

5.2 Results for seven categories of shapes

We experiment with 7 of the 10 categories of shapes shown in Figure 6 and the results are provided in Table 4. Similar to the results in Table 3, MDRG using eigenfunctions performs better than other techniques using HKS and WKS. Further, the results of the distance between MDRGs are comparable with that of MRSs using eigenfunctions and the bottleneck distance between Reeb graphs using SIHKS. This can be seen from the distance matrices shown in Figure 7. The proposed distance using MDRGs is better in discriminating different classes of shapes as compared to the distances based on Reeb graphs and MRSs.

6 CONCLUSION

In this article, we introduce a novel distance measure between MDRGs by computing the bottleneck distances for the component

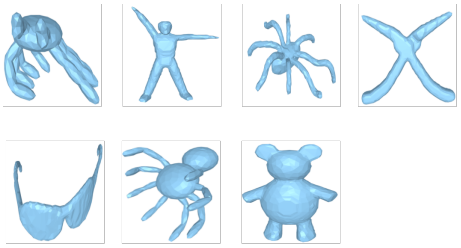

Figure 6: Seven categories of shapes from SHREC 2010.

Descriptors	Methods	NN	1-Tier	2-Tier	e-Measure	DCG
HKS	Histogram	0.9000	0.5534	0.7440	0.5174	0.8407
	MRS	0.9071	0.7658	0.9414	0.6709	0.9357
	PD of Reeb graph	0.9429	0.6335	0.7805	0.5683	0.8787
WKS	Histogram	0.9214	0.5470	0.7252	0.5087	0.8517
	MRS	0.9429	0.5703	0.7425	0.5199	0.8632
	PD of Reeb graph	0.8857	0.4523	0.6004	0.4171	0.7921
SIHKS	Histogram	0.9643	0.7868	0.9462	0.6818	0.9526
	MRS	0.9714	0.7992	0.9421	0.6801	0.9546
	PD of Reeb graph	0.9786	0.8105	0.9560	0.6849	0.9586
Pairs of Eigenfunctions	Histogram	0.9214	0.6898	0.8492	0.6059	0.9036
	MRS	0.9714	0.8477	0.9380	0.6882	0.9623
	PDs of MDRG	0.9571	0.8534	0.9278	0.6793	0.9633

Table 4: Performance Results for seven categories of shapes in SHREC 2010 dataset. Comparison of distance measures based on fiber-component distributions [2], MRSs [25], PDs of Reeb graphs [4] and PDs of MDRGs using HKS, WKS, SIHKS and pairs of eigenfunctions as shape descriptors.

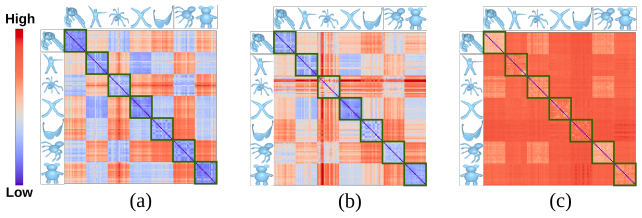

Figure 7: Distance matrices. (a) Bottleneck distance between Reeb graphs using SIHKS. (b), (c) Distances between MDRGs and MRSs, respectively using pairs of eigenfunctions.

Reeb graphs between the MDRGs. We show that the proposed distance measure is a pseudo-metric and satisfies the stability property. The effectiveness of the proposed distance measure is shown in the problem of shape matching, where the performance of using absolute of eigenfunctions as shape descriptors is compared with HKS, WKS and SIHKS.

The computation of the MDRG of a multi-field requires a JCN, which is computationally expensive to construct. Thus, there is a need for a faster algorithm for constructing the MDRG. We have shown an application of the proposed method in the problem of shape retrieval. However, exploring other computational domains will be useful for further analysis on the effectiveness of the proposed distance measure.

ACKNOWLEDGMENTS

The authors would like to thank the Science and Engineering Research Board (SERB), India (SERB/CRG/2018/000702) and International Institute of Information Technology (IIITB), Bangalore for funding this project and for generous travel support.

REFERENCES

[1] Pankaj Agarwal, Herbert Edelsbrunner, John Harer, and Yusu Wang. 2006. Extreme Elevation on a 2-Manifold. *Discrete & Computational Geometry* 36 (12 2006), 553–572. https://doi.org/10.1007/s00454-006-1265-8

[2] Tripti Agarwal, Amit Chattopadhyay, and Vijay Natarajan. 2019. Topological Feature Search in Time-Varying Multifield Data. *TopoInVis 2019, Nyköping, Sweden, preprint arXiv:1911.00687* (2019).

[3] Mathieu Aubry, Ulrich Schlickewei, and Daniel Cremers. 2011. The wave kernel signature: A quantum mechanical approach to shape analysis. *Proceedings of the IEEE International Conference on Computer Vision*, 1626–1633. https://doi.org/10.1109/ICCVW.2011.6130444

[4] Ulrich Bauer, Xiaoyin Ge, and Yusu Wang. 2014. Measuring Distance between Reeb Graphs. In *Proceedings of the Thirtieth Annual Symposium on Computational Geometry* (Kyoto, Japan) *(SOCG'14)*. Association for Computing Machinery, New York, NY, USA, 464–473.

[5] M. Bronstein and I. Kokkinos. 2010. Scale-invariant heat kernel signatures for non-rigid shape recognition. *2010 IEEE Computer Society Conference on Computer Vision and Pattern Recognition* (2010), 1704–1711.

[6] H. Carr and D. Duke. 2014. Joint Contour Nets. *IEEE Transactions on Visualization and Computer Graphics* 20, 8 (Aug 2014), 1100–1113. https://doi.org/10.1109/TVCG.2013.269

[7] Amit Chattopadhyay, Hamish Carr, David Duke, and Zhao Geng. 2014. Extracting Jacobi Structures in Reeb Spaces. In *EuroVis - Short Papers*, N. Elmqvist, M. Hlawitschka, and J. Kennedy (Eds.). The Eurographics Association, 1–4. https://doi.org/10.2312/eurovisshort.20141156

[8] Amit Chattopadhyay, Hamish Carr, David Duke, Zhao Geng, and Osamu Saeki. 2016. Multivariate topology simplification. *Computational Geometry: Theory and Applications* 58 (Oct. 2016), 1–24. https://doi.org/10.1016/j.comgeo.2016.05.006

[9] Isaac Chavel. 1984. *Eigenvalues in Riemannian geometry*. Academic press.

[10] Frédéric Chazal, David Cohen-Steiner, Marc Glisse, Leonidas J. Guibas, and Steve Y. Oudot. 2009. Proximity of Persistence Modules and Their Diagrams. In *Proceedings of the Twenty-Fifth Annual Symposium on Computational Geometry* (Aarhus, Denmark) *(SCG '09)*. Association for Computing Machinery, New York, NY, USA, 237–246. https://doi.org/10.1145/1542362.1542407

[11] David Cohen-Steiner, Herbert Edelsbrunner, and John Harer. 2007. Stability of Persistence Diagrams. *Discret. Comput. Geom.* 37, 1 (2007), 103–120.

[12] Tamal K. Dey, Facundo Mémoli, and Yusu Wang. 2016. Multiscale Mapper: Topological Summarization via Codomain Covers. In *Proceedings of the Twenty-Seventh Annual ACM-SIAM Symposium on Discrete Algorithms* (Arlington, Virginia) *(SODA '16)*. Society for Industrial and Applied Mathematics, USA, 997–1013.

[13] David Duke, Hamish Carr, Aaron Knoll, Nicolas Schunck, Hai Ah Nam, and Andrzej Staszczak. 2012. Visualizing Nuclear Scission through a Multifield Extension of Topological Analysis. *IEEE Transactions on Visualization and Computer Graphics* 18, 12 (2012), 2033–2040. https://doi.org/10.1109/TVCG.2012.287

[14] Herbert Edelsbrunner and John Harer. 2004. Jacobi Sets of Multiple Morse Functions. *Foundations of Computational Mathematics - FoCM* (01 2004).

[15] Herbert Edelsbrunner and John Harer. 2010. *Computational Topology - an Introduction*. American Mathematical Society. http://www.ams.org/bookstore-getitem/item=MBK-69

[16] Herbert Edelsbrunner, John Harer, and Amit K. Patel. 2008. Reeb Spaces of Piecewise Linear Mappings. In *Proceedings of the Twenty-Fourth Annual Symposium on Computational Geometry* (College Park, MD, USA) *(SCG '08)*. Association for Computing Machinery, New York, NY, USA, 242–250. https://doi.org/10.1145/1377676.1377720

[17] Herbert Edelsbrunner, David Letscher, and Afra Zomorodian. 2002. Topological Persistence and Simplification. *Discret. Comput. Geom.* 28, 4 (2002), 511–533. https://doi.org/10.1007/s00454-002-2885-2

[18] Masaki Hilaga, Yoshihisa Shinagawa, Taku Kohmura, and Tosiyasu L Kunii. 2001. Topology Matching for Fully Automatic Similarity Estimation of 3D Shapes. In *Proceedings of the 28th annual conference on Computer graphics and interactive techniques*. ACM, 203–212.

[19] Yanir Kleiman and Maks Ovsjanikov. 2017. Robust Structure-Based Shape Correspondence. *Computer Graphics Forum* 38 (10 2017).

[20] B. Levy. 2006. Laplace-Beltrami Eigenfunctions Towards an Algorithm That "Understands" Geometry. In *IEEE International Conference on Shape Modeling and Applications 2006 (SMI'06)*. 13–13. https://doi.org/10.1109/SMI.2006.21

[21] Chunyuan Li, Maks Ovsjanikov, and Frederic Chazal. 2014. Persistence-Based Structural Recognition. In *2014 IEEE Conference on Computer Vision and Pattern Recognition*. 2003–2010. https://doi.org/10.1109/CVPR.2014.257

[22] Zhouhui Lian, Afzal Godil, Thomas Fabry, Takahiko Furuya, Jeroen Hermans, Ryutarou Ohbuchi, Chang Shu, Dirk Smeets, Paul Suetens, Dirk Vandermeulen, and Stefanie Wuhrer. 2010. SHREC'10 track: Non-rigid 3D shape retrieval. 101–108. https://doi.org/10.2312/3DOR/3DOR10/101-108

[23] Diana Mateus, Fabio Cuzzolin, Radu Horaud, and Edmond Boyer. 2007. Articulated Shape Matching Using Locally Linear Embedding and Orthogonal Alignment. In *NRTL 2007 - Workshop on Non-rigid Registration and Tracking through Learning*. IEEE Computer Society Press, Rio de Janeiro, Brazil, 1–8. https://doi.org/10.1109/ICCV.2007.4409180

[24] Adrien Poulenard, Primoz Skraba, and Maks Ovsjanikov. 2018. Topological Function Optimization for Continuous Shape Matching. *Computer Graphics Forum* 37 (08 2018), 13–25.

[25] Yashwanth Ramamurthi, Tripti Agarwal, and Amit Chattopadhyay. 2021. A Topological Similarity Measure between Multi-resolution Reeb Spaces. *IEEE Transactions on Visualization and Computer Graphics* (2021), 1–1. https://doi.org/10.1109/TVCG.2021.3087273

[26] Martin Reuter, Franz-Erich Wolter, and Niklas Peinecke. 2006. Laplace-Beltrami Spectra as 'Shape-DNA' of Surfaces and Solids. *Comput. Aided Des.* 38, 4 (apr 2006), 342–366. https://doi.org/10.1016/j.cad.2005.10.011

[27] Martin Reuter, Franz-Erich Wolter, Martha Shenton, and Marc Niethammer. 2009. Laplace–Beltrami eigenvalues and topological features of eigenfunctions for statistical shape analysis. *Computer-Aided Design* 41, 10 (2009), 739–755. https://doi.org/10.1016/j.cad.2009.02.007

[28] Steven Rosenberg. 1997. *The Laplacian on a Riemannian Manifold: An Introduction to Analysis on Manifolds*. Cambridge University Press. https://doi.org/10.1017/CBO9780511623783

[29] Raif M. Rustamov. 2007. Laplace-Beltrami Eigenfunctions for Deformation Invariant Shape Representation. In *Geometry Processing*, Alexander Belyaev and Michael Garland (Eds.). The Eurographics Association. https://doi.org/10.2312/SGP/SGP07/225-233

[30] Raif M. Rustamov. 2007. Laplace-Beltrami Eigenfunctions for Deformation Invariant Shape Representation. In *Geometry Processing*, Alexander Belyaev and Michael Garland (Eds.). The Eurographics Association. https://doi.org/10.2312/SGP/SGP07/225-233

[31] Osamu Saeki. 2004. *Topology of singular fibers of differentiable maps*. Lecture Notes in Mathematics, Vol. 1854. Springer Heidelberg, Germany.

[32] Osamu Saeki. 2017. Theory of Singular Fibers and Reeb Spaces for Visualization. In *Topological Methods in Data Analysis and Visualization IV*, Hamish Carr, Christoph Garth, and Tino Weinkauf (Eds.). Springer International Publishing, Cham, 3–33.

[33] Osamu Saeki, Shigeo Takahashi, Daisuke Sakurai, Hsiang-Yun Wu, Keisuke Kikuchi, Hamish Carr, David Duke, and Takahiro Yamamoto. 2014. *Visualizing Multivariate Data Using Singularity Theory*. Mathematics for Industry, Vol. 1. Springer Japan, Chapter The Impact of Applications on Mathematics, 51–65.

[34] Gurjeet Singh, Facundo Mémoli, and Gunnar E. Carlsson. 2007. Topological Methods for the Analysis of High Dimensional Data Sets and 3D Object Recognition. In *PBG@Eurographics*.

[35] Raghavendra Sridharamurthy, Talha Bin Masood, Adhitya Kamakshidasan, and Vijay Natarajan. 2020. Edit Distance between Merge Trees. *IEEE Transactions on Visualization and Computer Graphics* 26, 3 (2020), 1518–1531. https://doi.org/10.1109/TVCG.2018.2873612

[36] Jian Sun, Maks Ovsjanikov, and Leonidas Guibas. 2009. A Concise and Provably Informative Multi-Scale Signature Based on Heat Diffusion. In *Proceedings of the Symposium on Geometry Processing* (Berlin, Germany) *(SGP '09)*. Eurographics Association, Goslar, DEU, 1383–1392.

[37] Gary K. L. Tam and Rynson W. H. Lau. 2007. Deformable Model Retrieval Based on Topological and Geometric Signatures. *IEEE Transactions on Visualization and Computer Graphics* 13, 3 (May 2007), 470–482.

[38] Junyi Tu, Mustafa Hajij, and Paul Rosen. 2019. Propagate and Pair: A Single-Pass Approach to Critical Point Pairing in Reeb Graphs. In *Advances in Visual Computing*, George Bebis, Richard Boyle, Bahram Parvin, Darko Koracin, Daniela Ushizima, Sek Chai, Shinjiro Sueda, Xin Lin, Aidong Lu, Daniel Thalmann, Chaoli Wang, and Panpan Xu (Eds.). Springer International Publishing, 99–113.

[39] S. Umeyama. 1988. An eigendecomposition approach to weighted graph matching problems. *IEEE Transactions on Pattern Analysis and Machine Intelligence* 10, 5 (1988), 695–703. https://doi.org/10.1109/34.6778

[40] Zihao Wang and Hongwei Lin. 2020. 3D shape retrieval based on Laplace operator and joint Bayesian model. *Visual Informatics* 4, 3 (2020), 69–76. https://doi.org/10.1016/j.visinf.2020.08.002

[41] Xiaoyu Zhang, Marcos, Chandrajit L. Bajaj, and Nathan Baker. 2004. Fast Matching of Volumetric Functions Using Multi-resolution Dual Contour Trees.

[42] Afra Zomorodian and Gunnar Carlsson. 2005. Computing Persistent Homology. *Discrete Comput. Geom.* 33, 2 (feb 2005), 249–274.

A STABILITY OF THE MDRG WITH RESPECT TO THE PROPOSED DISTANCE MEASURE

In this section we prove that the MDRG structure is stable with respect to the proposed distance measure. Let $\mathbf{f} = (f_1, f_2) : \mathbb{M} \to \mathbb{R}^2$ and $\mathbf{g} = (g_1, g_2) : \mathbb{M} \to \mathbb{R}^2$ be two bivariate fields defined on a compact metric space $\mathbb{M}$ such that f_1, f_2, g_1 and g_2 are tame functions. Let $\mathbb{MR}_{\mathbf{f}}$ and $\mathbb{MR}_{\mathbf{g}}$ be the MDRGs of $\mathbf{f}$ and $\mathbf{g}$, respectively. Then we prove the following lemma.

Lemma A.1.

$$d^0_{\mathbb{MR}}(\mathbb{MR}_{\mathbf{f}}, \mathbb{MR}_{\mathbf{g}}) \leq ||f_1 - g_1||_\infty + \frac{1}{2}\max\{Amp(f_2), Amp(g_2)\}$$

where $Amp(f)$ denotes the amplitude of a real-valued function $f : \mathbb{M} \to \mathbb{R}$ and is defined as follows:

$$Amp(f) = \max_{x\in\mathbb{M}} f(x) - \min_{y\in\mathbb{M}} f(y).$$

Proof. The term $d_B\left(\mathrm{PD}_0\left(\mathcal{RG}_{f_1}\right), \mathrm{PD}_0\left(\mathcal{RG}_{g_1}\right)\right)$ in $d^0_{\mathbb{MR}}(\mathbb{MR}_{\mathbf{f}}, \mathbb{MR}_{\mathbf{g}})$ of equation (10) is bounded above by $||f_1 - g_1||_\infty$ (see [11] for more details). We now prove a bound on the term $\int\limits_{c\in R(f_1,g_1)} \inf\limits_{\psi:\mathbb{S}^c_{f_1}\to\mathbb{S}^c_{g_1}} \sup\limits_{\mathcal{RG}\in\mathbb{S}^c_{f_1}} d_B\left(\mathrm{PD}_0\left(\mathcal{RG}\right), \mathrm{PD}_0\left(\psi\left(\mathcal{RG}\right)\right)\right)$.

Let $\mathcal{RG} \in \mathbb{S}^c_{f_1}$. Now, every point in the persistence diagram $\mathrm{PD}_0\left(\mathcal{RG}\right)$ corresponds to a 0-dimensional class whose birth and death lies between $\min\limits_{x\in\mathcal{RG}} \overline{\overline{f_2^p}}(x)$ and $\max\limits_{x\in\mathcal{RG}} \overline{\overline{f_2^p}}(x)$. Therefore, the maximum persistence of a point in $\mathrm{PD}_0\left(\mathcal{RG}\right)$ is at most the amplitude of $\overline{\overline{f_2^p}}$ in $\mathcal{RG}$.

$$\begin{aligned}\max_{x\in\mathrm{PD}_0(\mathcal{RG})} pers(x) &\leq \max_{p\in\mathcal{RG}_{\overline{\overline{f_2^p}}}} \overline{\overline{f_2^p}}(p) - \min_{p\in\mathcal{RG}_{\overline{\overline{f_2^p}}}} \overline{\overline{f_2^p}}(p).\\ &\leq \max_{p\in\mathbb{M}} f_2(p) - \min_{p\in\mathbb{M}} f_2(p).\\ &= Amp(f_2). \end{aligned} \tag{15}$$

Similarly, for $\mathcal{RG}' \in \mathbb{S}^c_{g_2}$, the following bound is obtained on the maximum persistence of a point in the persistence diagram $\mathrm{PD}_0\left(\mathcal{RG}'\right)$.

$$\max_{x\in\mathrm{PD}_0(\mathcal{RG}')} pers(x) \leq Amp(g_2). \tag{16}$$

Let $(a, b) \in \mathrm{PD}_0(\mathcal{RG})$ and (c, d) be its matching pair in $\mathrm{PD}_0(\mathcal{RG}')$ corresponding to $d_B\left(\mathrm{PD}_0\left(\mathcal{RG}\right), \mathrm{PD}_0\left(\mathcal{RG}'\right)\right)$. Then $||(a, b) - (c, d)||_\infty$ is at most $\max\{\frac{a+b}{2}, \frac{c+d}{2}\}$. Otherwise, we can match (a, b) to $(\frac{a+b}{2}, \frac{a+b}{2})$, (c, d) to $(\frac{c+d}{2}, \frac{c+d}{2})$ and obtain the required bound. Therefore, for any matched pair of points (x, x'), $||x - x'||_\infty$ is bounded by $\max\{\frac{1}{2}pers(x), \frac{1}{2}pers(x')\}$. We now obtain a bound on $d_B\left(\mathrm{PD}_0\left(\mathcal{RG}\right), \mathrm{PD}_0\left(\mathcal{RG}'\right)\right)$ as follows:

$$\begin{aligned} &d_B\left(\mathrm{PD}_0\left(\mathcal{RG}\right), \mathrm{PD}_0\left(\mathcal{RG}'\right)\right)\\ &\leq \max\left\{\max_{x\in\mathrm{PD}_0(\mathcal{RG})} \frac{1}{2}pers(x), \max_{x\in\mathrm{PD}_0(\mathcal{RG}')} \frac{1}{2}pers(x)\right\}\\ &\leq \frac{1}{2}\max\{Amp(f_2), Amp(g_2)\}\\ &\qquad \text{(from equations (15) and (16)).} \end{aligned}$$

$$\begin{aligned} &d^0_{\mathbb{MR}}(\mathbb{MR}_{\mathbf{f}}, \mathbb{MR}_{\mathbf{g}})\\ &= d_B\left(\mathrm{PD}_0\left(\mathcal{RG}_{f_1}\right), \mathrm{PD}_0\left(\mathcal{RG}_{g_1}\right)\right) +\\ &\quad \frac{1}{|R(f_1,g_1)|}\int\limits_{c\in R(f_1,g_1)} \inf_{\psi:\mathbb{S}^c_{f_1}\to\mathbb{S}^c_{g_1}} \sup_{\mathcal{RG}\in\mathbb{S}^c_{f_1}} d_B\left(\mathrm{PD}_0\left(\mathcal{RG}\right), \mathrm{PD}_0\left(\psi\left(\mathcal{RG}\right)\right)\right)\\ &\leq ||f_1 - g_1||_\infty + \frac{1}{|R(f_1,g_1)|}\int\limits_{c\in R(f_1,g_1)} \frac{1}{2}\max\{Amp(f_2), Amp(g_2)\}.\\ &= ||f_1 - g_1||_\infty + \frac{1}{2}\max\{Amp(f_2), Amp(g_2)\}. \end{aligned}$$

□

Lemma A.2.

$$d^1_{\mathbb{MR}}(\mathbb{MR}_{\mathbf{f}}, \mathbb{MR}_{\mathbf{g}}) \leq 3||f_1 - g_1||_\infty + \frac{1}{2}\max\{Amp(f_2), Amp(g_2)\}.$$

Proof. The term $d_B\left(ExPD_0\left(\mathcal{RG}_{f_1}\right), ExPD_0\left(\mathcal{RG}_{g_1}\right)\right)$ in $d^1_{\mathbb{MR}}(\mathbb{MR}_{\mathbf{f}}, \mathbb{MR}_{\mathbf{g}})$ is bounded above by $3||f_1 - g_1||_\infty$ (see Theorems 4.1 and 4.3 in [4] for more details). The rest of the proof is similar to that of Lemma A.1. □

The following theorem gives the stability of $d_T(\mathbb{MR}_{\mathbf{f}}, \mathbb{MR}_{\mathbf{g}})$.

Theorem A.3. ***Stability:***

$$d_T(\mathbb{MR}_{\mathbf{f}}, \mathbb{MR}_{\mathbf{g}}) \leq 3||f_1 - g_1||_\infty + \frac{1}{2}\max\{Amp(f_2), Amp(g_2)\}.$$

Proof.

$$\begin{aligned} &d_T(\mathbb{MR}_{\mathbf{f}}, \mathbb{MR}_{\mathbf{g}})\\ &= w_0 \cdot d^0_{\mathbb{MR}}(\mathbb{MR}_{\mathbf{f}}, \mathbb{MR}_{\mathbf{g}}) + w_1 \cdot d^0_{\mathbb{MR}}(\mathbb{MR}_{-\mathbf{f}}, \mathbb{MR}_{-\mathbf{g}}) +\\ &\qquad w_2 \cdot d^1_{\mathbb{MR}}(\mathbb{MR}_{\mathbf{f}}, \mathbb{MR}_{\mathbf{g}})\\ &\leq w_0\left(||f_1 - g_1||_\infty + \frac{1}{2}\max\{Amp(f_2), Amp(g_2)\}\right) +\\ &\quad w_1\left(||f_1 - g_1||_\infty + \frac{1}{2}\max\{Amp(f_2), Amp(g_2)\}\right) +\\ &\quad w_2\left(3||f_1 - g_1||_\infty + \frac{1}{2}\max\{Amp(f_2), Amp(g_2)\}\right)\\ &\qquad \text{(using Lemmas A.1, A.2)}\\ &\leq 3||f_1 - g_1||_\infty + \frac{1}{2}\max\{Amp(f_2), Amp(g_2)\}\\ &\qquad \text{(since } w_0 + w_1 + w_2 = 1\text{).} \end{aligned}$$

□